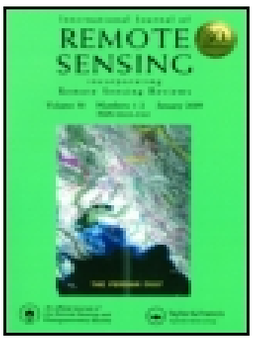

International Journal of Remote Sensing

ISSN: 0143-1161 (Print) 1366-5901 (Online) Journal homepage: http://www.tandfonline.com/loi/tres20

Remote sensing of the impacts of construction in coastal waters on suspended particulate matter concentration – the case of the Yangtze River delta, China

Lina Cai, Danling Tang, Gad Levy & Dongyan Liu

To cite this article: Lina Cai, Danling Tang, Gad Levy & Dongyan Liu (2015): Remote sensing of the impacts of construction in coastal waters on suspended particulate matter concentration – the case of the Yangtze River delta, China, International Journal of Remote Sensing, DOI: 10.1080/01431161.2015.1121302

To link to this article: http://dx.doi.org/10.1080/01431161.2015.1121302

International Journal of Remote Sensing, 2015
http://dx.doi.org/10.1080/01431161.2015.1121302

Taylor & Francis
Taylor & Francis Group

Remote sensing of the impacts of construction in coastal waters on suspended particulate matter concentration – the case of the Yangtze River delta, China

Lina Cai[a,b,c], Danling Tang[b,c,d]*, Gad Levy[b,e], and Dongyan Liu[d,f]

[a]*School of Marine Sciences, ZheJiang Ocean University, ZhouShan, ZheJiang 316022, China;* [b]*Research Centre for Remote Sensing of Marine Ecology & Environment, State Key Laboratory of Tropical Oceanography, South China Sea Institute of Oceanology, Chinese Academy of Sciences, Guangzhou 510301, China;* [c]*School of Ocean Sciences, University of Chinese Academy of Sciences, Beijing, 100049, China;* [d]*Collaborative Innovation Centre for 21st-Century Maritime Silk Road Studies, Guangzhou, China;* [e]*NorthWest Research Associates, Seattle, WA 98052, USA;* [f]*Yantai Institute of Costal Zone Research, Chinese Academy of Sciences, Yantai 264003, China*

(*Received 24 January 2015; accepted 2 November 2015*)

This study investigates the capability of high-spatial resolution Landsat Thematic Mapper (TM) data to sense and document suspended particulate matter concentration (SPMC) variability resulting from the influence of large structures in coastal waters. Two bridges, located in the coastal waters of the Yangtze River delta, are used as examples. A new SPMC inverse model, relating SPMC to TM optical properties through linear regression in the red and near-infrared bands, is developed. In total, 780 samples and 30 transects taken between 2006 and 2011 were used to compare and contrast SPMC at locations upstream and downstream of the bridges. The comparisons show: (i) within a distance of 0.3 km downstream from the bridges, SPMC mostly increased by 3–60% (8.40–176.29 mg l^{-1}); (ii) when SPMC values upstream were low (<300 mg l^{-1}), the increase in SPMC extended to 3.0–6.5 km downstream; (iii) under conditions of high turbidity (>400 mg l^{-1}) upstream, decreases in SPMC were observed in 0.3–6.5 km downstream. The bridges influenced SPMC by blocking the transport of upstream suspended particulate matter (deposition) and through stirring of the sediments near the base of their piers (resuspension). The results can be generalized to other offshore engineering structures.

1. Introduction

Suspended particulate matter (SPM) has significant impacts on the marine environment. The Yangtze River transports several hundred million tonnes of SPM per year (Chen, Zhang, and Yang 2003), some of which enter Hangzhou Bay (Jilan and Kangshan 1989; Tang et al. 1998). The turbidity in Hangzhou Bay depends mainly upon the remote sediments supplied by the near-shore coastal currents and tidal currents, as well as on internal sediment resuspension (Chen and Wang 2008). The SPM in Hangzhou Bay is transported mainly by advection, mixing, and settling (Hu et al. 2009), affecting transparency, turbidity, water quality, and geomorphology (Cloern 1987; Mayer et al. 1998; Tang et al. 2003a; Webster and Lemckert 2002).

*Corresponding author. Email: lingzistdl@126.com

Table 1. Hangzhou Bay bridge (HBB) and Jin Tang bridge (JTB).

Bridge	Construction date	Length (km)	Average pier spacing (m)	Reason for construction	Approximate water blockage (%)
HBB	2003–2007	36.00	60.00	To shorten the coastal transport route	5–9
JTB	2006–2009	18.50	52.86	To provide access to Jin Tang and other islands	5–9

Numerous near-shore constructions that can affect the ecology and geomorphology of bays have been built in recent years. Two such constructions, which are studied here, are large bridges (Table 1) in the Yangtze River delta. The first is Hangzhou Bay bridge (HBB, Figure 1(*c*)), opened in 2007, which spans the main channel of the bay connecting Jiaxing and Cixi, near Ningbo. The second of these, Jin Tang bridge (JTB, Figure 1(*d*)), which connects Zhenhai and Jin Tang Island, was opened in 2009.

Experimental and numerical simulation studies have been conducted to investigate how bridges affect the flow dynamics and impact the local ocean environment (Liu 2006; Shin and Park 2010). Prior studies have found that bridge piers generate horseshoe vortex systems (Unger and Hager 2007) and affect equilibrium scour

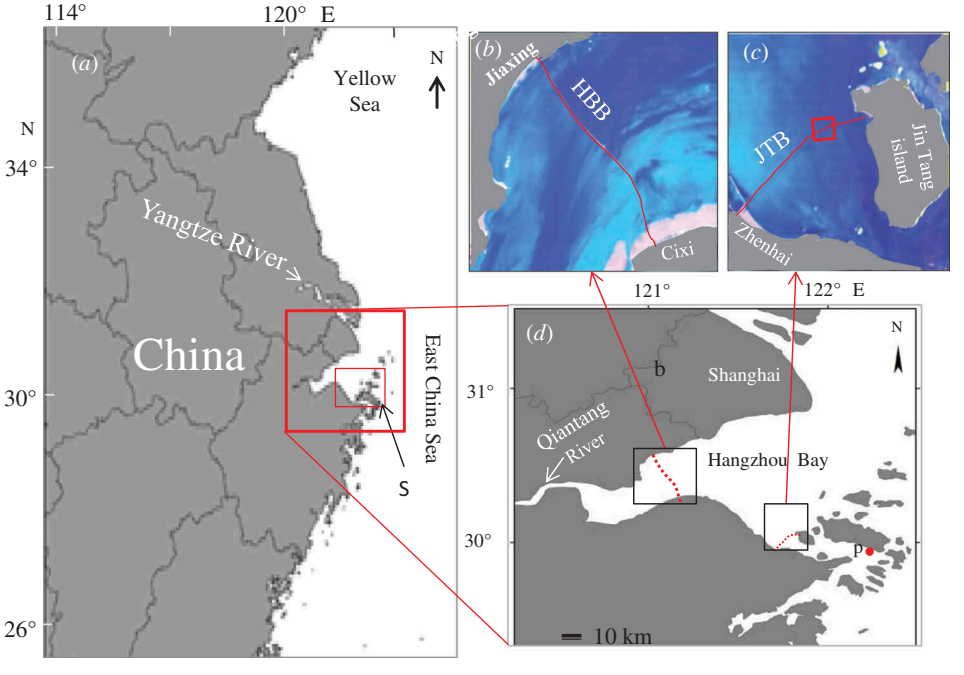

Figure 1. (*a*) Location of coastal waters in Yangtze River delta. (*b*) and (*c*) HBB and JTB. (*d*) Location of HBB and JTB on the map of the study area. Small red square area (S): The location of the *in situ* sampling area. Red square in (*d*): the location of the region of Figure 2(*c*). Red point p: the location of the open-air ocean water pool.

depth, which are dependent upon the characteristics of both the fluid and bed sediments, pier geometry, and Reynolds number (Baker 1979; Firat and Gungor 2009; Pasiok and Stilger-SzydŁO 2010; Raudkivi and Ettema 1983; Ting et al. 2001; Unger and Hager 2007). Another study found that the equilibrium scour in clay is about the same as in sand, but the rates of scour are much slower in the former (Ting et al. 2001). One numerical study showed the obstruction impact of a bridge on sediment transport at the mouth of Hangzhou Bay (Qiao et al. 2011). Due to lack of observational data, however, very few remote-sensing-based studies have focused on the impacts of major offshore constructions, especially bridges across a bay, on SPM transport and distribution.

Much research has been done on SPM monitoring using remote-sensing data. Since 1978, the Coastal Zone Color Scanner (CZCS) and other satellite ocean colour sensors have been used to monitor SPM and chlorophyll-*a* in China's coastal waters (Li and Guo 2014; Shen et al. 2010; Tang et al. 1998; Zhang et al. 2014). Based on the relationship between SPMC and reflectance, remote-sensing data can be used to interpret ocean sedimentary information (Fan, Huang, and Tang 2007; MatAmin et al. 2012; Qiu 2013; Tang et al. 2003b), such as total suspended matter (TSM), suspended sediment concentration, and SPM direction (Chen and Wang 2008; Choi et al. 2014; He et al. 2013; Shen et al. 2010; Zhang et al. 2014).

In recent decades, local marine environment monitoring applications have used high-spatial resolution satellite remote-sensing data acquired from Landsat Thematic Mapper (TM) and the Advanced Spaceborne Thermal Emission and Reflection Radiometer (ASTER). These data clearly show detailed information on water bodies (Charou et al. 2010). The influence of suspended sediment particles on water spectral characteristics was also analysed (Cai, Tang, and Li 2015a; Dekker, Vos, and Peters 2002; Doxaran, Cherukuru, and Lavender 2006; Zhou et al. 2006), and it was found that the sensitivity of particular wavelength bands to SPM varies with water constituents.

This study investigates the influence of major offshore constructions, specifically bridges across a bay, on SPM transport and distribution using high-spatial resolution data through quantitative and qualitative analysis of SPMC variation. It documents in detail the impacts of the bridges on the movement and distribution of SPM in the vicinity of the bridges from a remote-sensing perspective.

2. Data and methods

2.1. Study area

Hangzhou Bay and Jin Tang bridges are located in Hangzhou Bay, a funnel-shaped bay with an average depth of around 9 m at low tide (Liu et al. 2012; Wang et al. 2012; Xie et al. 2009), in the coastal waters of the Yangtze River delta, in the East China Sea, 29–32° N and 120–123° E (Figure 1(*a*) and (*b*)). The topography of Hangzhou Bay includes shallow shoals to the northeast, a deep tidal channel with a maximum depth of 13 m along the northern bank (He et al. 2013), tidal channel sand ridges in the middle, and large sandbar areas in the south. Hangzhou Bay is influenced by Yangtze River estuary south-flowing water, Qiantang River runoff, and East China Sea tidal flow, leading to strong tides, rapid flow, and high SPMC there (Cai et al. 2015b; Shengquan, Guohui, and Yuhen 1993; Jilan and Kangshan 1989).

2.2. Field data collection

Two field data collection campaigns were conducted in 2009 and 2014 (denoted by small red square (S) in Figure 1(*a*); (Table 2). The first survey collected water samples from 62 stations at around 10:15 on 17 July 2009 using 10 fishing boats at different positions in the sampling area (S in Figure 1(*a*)); their locations were changed and water samples were collected about 300 m apart between 9:45 and 10:45, giving a total of 62 water samples used in this study. The SPMC values of the water samples were measured in the laboratory: 27 were used to construct an SPMC inverse model based on satellite data obtained synchronously, with the remaining 35 used to validate the model.

To study the changes in spectral characteristics induced by SPM and determine the wave bands sensitive to changes in SPMC, a second survey was conducted on 30 March 2014, from 8:00–16:00. The remote-sensing reflectance (R_{rs}) and SPMC were synchronously measured. A set of experimental data (15 samples) of low SPMC was retrieved on 10 April 2014 (14:30–16:00) from an open-air ocean water pool whose position is shown in Figure 1(*b*) (red point, p). The depth of the pool was around 6 m; the bottom was not visible during measurement because of SPM.

The R_{rs} value was detected using an ISI921VF visible, near-infrared (NIR) spectral radiometer with a spectral range of 380–1080 nm.

The measured R_{rs} is calculated from Equation (1):

$$R_{rs} = \frac{L_w - \rho L_s}{\pi L_p / \rho_p}, \tag{1}$$

where L_w is the radiance received by the ISI921VF above the sea–water surface; L_s is the radiance of the sky; ρ_p is the reflectance of the plate; L_p is the radiance received by the ISI921VF above the plate; and ρ is the dimensionless air–water reflectance and is always in the range 0.022–0.050. ρ is calculated assuming a black ocean at wavelengths from 1000 to 1020 nm (Hale and Querry 1973) and wavelength independence (Doxaran et al. 2002).

The SPMC was defined as the dry mass of particles per unit volume of water (mg l^{-1}). The water samples were taken below the sea surface, simultaneously with *in situ* optical measurements. To obtain the SPMC values, the water samples were first filtered and the filters were then dried for 24 hours at 40ºC and reweighed (Qiu 2013). The salinity of Hangzhou Bay water is nearly half that of ocean water, and thus contributes to gravimetric SPM measurement if salt is not properly washed out. In this scenario it might not play any role because the overall level of SPM is very high, so that the contribution of salt in the dried filters can be ignored.

Table 2. *In situ* measurements.

Survey	Location	No. of measurement stations	Time	Measurements taken
1	30.37°–30.65°N, 121.25°–122°E	62	9:45–10:45 on 17 July 2009	SPMC
2	29.91°–29.98°N, 122.17°–122.22°E	30	8:00–16:00 on 30 March 2014	SPMC, R_{rs}

2.3. Remote-sensing data and data processing

Eleven Landsat-5 TM images were used for this study, two in each of the years 2006 to 2010 and one in 2011, all acquired under clear sky conditions between 10:13 and 10:20 local time. The dates were 3 March and 20 April 2006, 2 February and 28 July 2007, 24 March and 11 May 2008, 28 April and 17 July 2009, 9 November and 27 December 2010, and 23 July 2011.

Geometric correction was performed in this study to eliminate geometric distortion in satellite images, by referencing a topographic map of Hangzhou Bay area (Dewidar and Khedr 2001). A polynomial geometric correction model, which has been widely used for satellite image correction, was used (Hadjimitsis et al. 2006) and the root mean square error (RMSE) for positional accuracy was generally less than 0.5 pixels.

A dark pixel subtraction method was applied for atmospheric correction (Chavez Jr 1988; Mustak 2013; Pattiaratchi et al. 1994; Warrick et al. 2004) to eliminate atmospheric distortion due to atmospheric absorption and scattering of electromagnetic radiation from Landsat-5 TM data (Hu et al. 2004). Land-based clear water bodies (e.g. clear lake waters here) were used as standard reflectors for atmospheric measurements (Teillet and Fedosejevs 1995). The standard reflectors (dark objects) can be found in the three continuous images (covering Hangzhou Bay water along with surrounding lakes, rivers, and some other land information), with the middle one covering Hangzhou Bay and the two adjacent images lying immediately ahead and behind it on the same orbit (Cai, Tang, and Li 2015a).

Atmospheric contribution in each band was assumed to be the difference between the reflectance at the top of the atmosphere and that of dark objects. In prior studies, clear lake water surface reflectance in TM red and NIR bands was found to be 0.03 and 0.01, respectively (Richter 1990; Teillet and Fedosejevs 1995). Atmospheric correction was performed following the procedure of Zhou et al. (2006). The first step was to convert the image's original pixel value to the top-of-atmosphere reflectance. Then, the histogram method was used to identify pixels of clear waters from the images by selecting the lower bound of the histogram in TM band 4. The third step, subtraction of the reflectance contributed by the atmosphere, was finally conducted for each band.

A comparative analysis of the two sides of both bridges was conducted for every image. The sub-zenith angle remained the same for all images.

Seven hundred and eighty paired points were sampled along the bridges from 11 landsat-5 TM images, with one point sampled upstream close to the bridges and its pair sampled downstream along the streamline, within 0.3 km away from the bridges. These paired points were evenly sampled from water containing different SPMC values in the study area around the the bridges.

Furthermore, we measured SPMC along 30 transects, aligned normal to the bridges, to compare the SPMC on opposite sides of the bridges.

2.4. Water current simulation

Hangzhou Bay tidal currents were simulated using the Regional Ocean Modelling System (ROMS) (Rutgers version 3.2, Song and Haidvogel (1994), see http://www.myroms.org/). The bottom topography was extracted from the topographic data set ETOPO1 (Amante and Eakins 2009), and the air–sea heat flux and wind stress data were obtained from NCEP/DOE Reanalysis 2 (Prasad and Singh 2009). In this study we aimed to determine the current fields in the water surrounding the bridges, which occupy an area much wider than that of the bridge, in order to estimate the effects of the bridges on suspended sediment variability. In

this case, the numerical model (ROMS) was used to provide a reliable current estimate even though the resolution of the model is lower than the scale of a bridge. Furthermore, the model results were well validated (Fan and Song 2014).

3. Results

3.1. Changes in water spectral characteristics

Two reflectance peaks (Figure 2(*a*)) were found from the *in situ*-measured reflectance curves (for SPMC >150 mg l^{-1}), in the ranges 630–730 nm and 770–850 nm. The values of the two reflectance peaks are therefore close. The experimental reflectance curves (Figure 2(*b*)) obtained from the low-SPMC water pool (for SPMC <100 mg l^{-1})

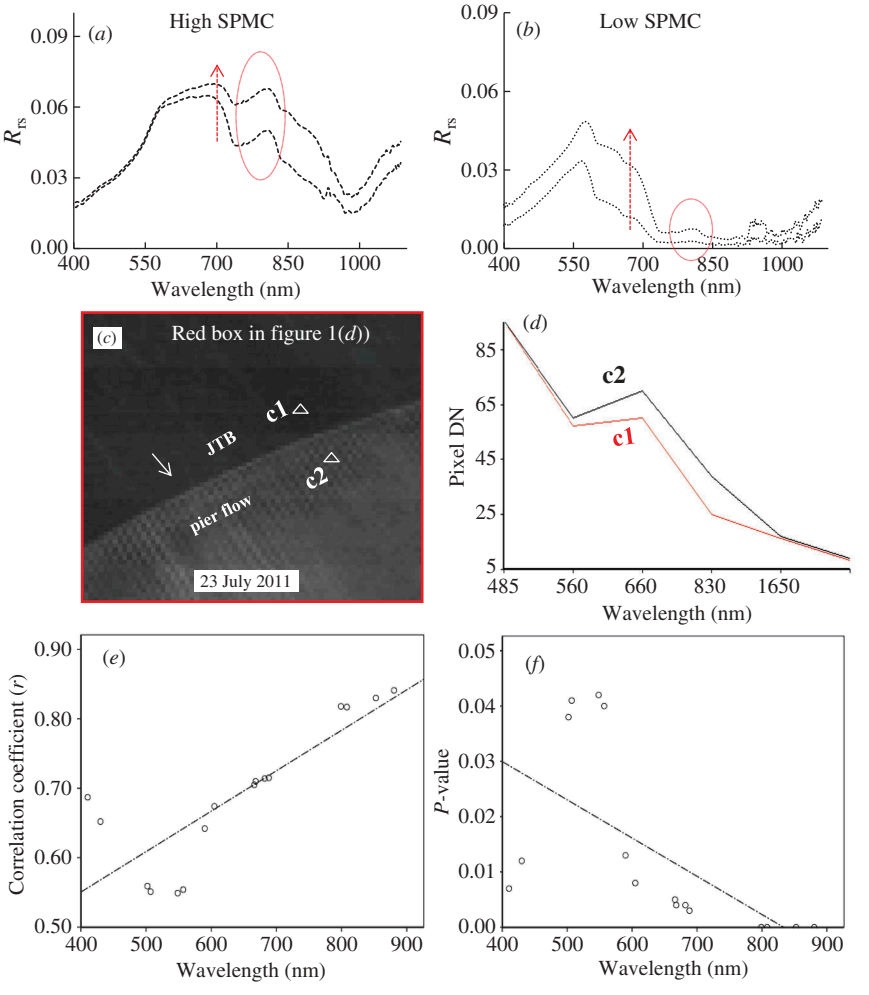

Figure 2. Spectral reflectance curves of sampled points in Hangzhou Bay area sampled from (*a*) Hangzhou Bay and (*b*) experimenal water). (*c*) Pier-induced comb flow and location of sampling points (c1–c2). (*d*) Spectral profiles (c1–c2) of sampling points in (*c*). (*e*) Change in the value of the correlation coefficient between SPMC and R_{rs} with wavelength. (*f*) Change in the *p*-value from the correlation analysis of SPMC and R_{rs} with wavelength.

show two reflectance peaks, with a major one around 570 nm and a weak one around 800 nm. An increasing trend with increasing SPMC can be seen in the reflectance of the red (red arrows in Figure 2(*a*) and (*b*)) and NIR bands (red circles in Figure 2(*a*) and (*b*)).

Spectral profile curves acquired from Landsat TM images on opposite sides of the bridges show distinct differences in the red and NIR bands, with the values of point c1 lower than those of point c2 in Figure 2(*c*) and (*d*).

3.2. *A new SPMC estimation model: 'SPM-CT'*

Water spectral analysis and correlation analysis were carried out to determine the relationship between SPMC and reflectance as a function of wavelength. A linear regression analysis between SPMC and R_{rs} at different wavelengths was conducted and a linear correlation was calculated. The highest correlation between SPMC and R_{rs} was found in the NIR band as compared with the blue, green, and red bands, with a correlation coefficient in the range 0.77–0.86 ($P < 0.005$) (panels (*e*) and (*f*) in Figure 2). The red band follows the NIR band, presenting a secondary correlation with the SPMC in water of high turbidity water. The red band (red arrow in Figure 2(*b*)) is more sensitive to suspended sediment than the NIR band in water of low SPMC. Therefore, the NIR band (TM band 4) and red band (TM band 3) were adopted to establish an model for estimation of SPMC.

Nine pixel values (i.e. calibrated reflectance in the fourth and third bands – R_4 and R_3) around each sampling site were first averaged and then used to establish the regression model. The linear regression relationship between the averaged R_4, R_3 reflectance and the actual SPMC values was derived (Equation (2), with R^2 0.976, $P < 0.005$) using the *in situ* data set. The data set contained 27 water samples, with SPMC values ranging from 179 to 616 mg l^{-1}, and a mean value of 389.58 mg l^{-1}. The new model, named 'SPM-CT' (C: Cai; T: Tang) (Equation (2)) is:

$$S_{PMC} = 314.435 \times R_3 + 3805.982 \times R_4 + 28.54, \tag{2}$$

where S_{PMC} is the suspended particulate matter concentration (mg l^{-1}) and R_3, R_4 denote the calibrated reflectance (i.e. after applying atmosphere correction) in the third (red) and fourth (NIR) bands, respectively.

The calculations were performed with software ENVI 4.5 (ENVI 1997).

To further understand the applicability of 'SPM-CT', we evaluated its performance using a validation data set of 35 samples. These 35 test cases are from different locations and are independent from the 27 data points used to determine the regression coefficients. Comparisons between *in situ* SPMC and model-estimated values showed close agreement (Figure 3), with a highly significant linear relationship and a coefficient of determination, R^2, of 0.978 ($P < 0.005$). The 'SPM-CT' model is, therefore, suitable for comparison of SPMC on opposite sides of the bridge.

3.3. *Model-retrieved SPMC*

3.3.1. *SPMC distribution in the vicinity of the bridges*

The distribution of SPMC (Figure 4(*a*)–(*c*)) in the research area was retrieved from 11 TM images (here we take three images for 28 July 2007, 17 July 2009, and 23

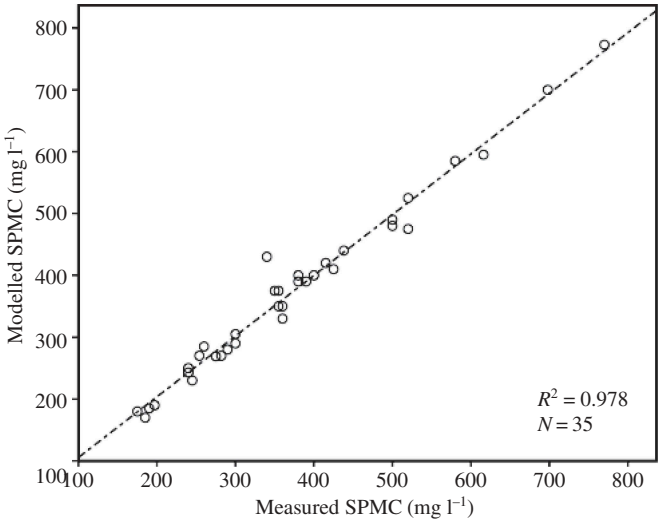

Figure 3. Regressions of the measured SPMC and estimated SPMC from 'SPM-CT' model.

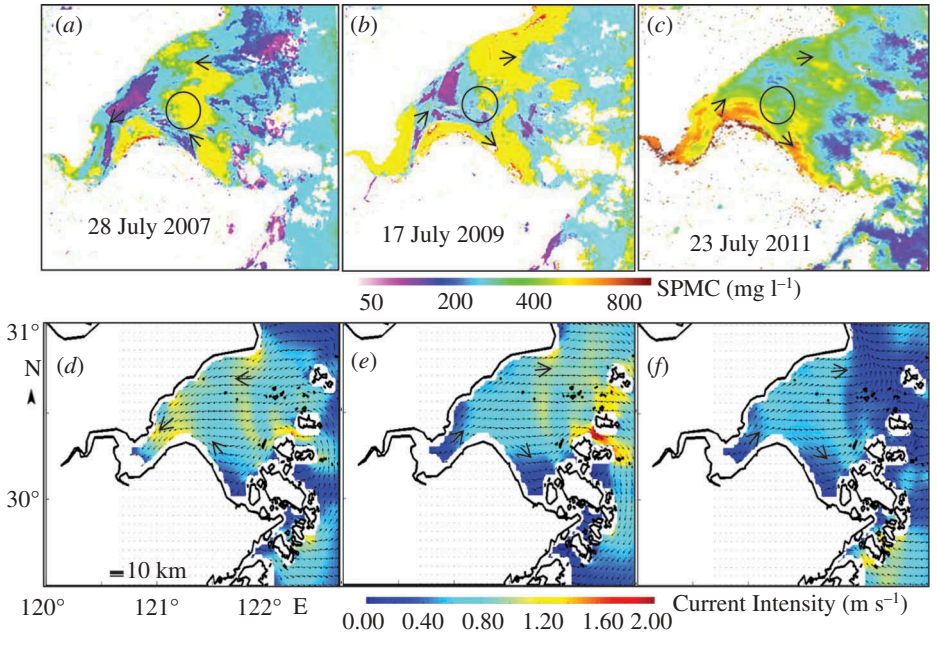

Figure 4. Surface SPMC retrieved from Landsat TM images around 10:15 on 28 July 2007 (*a*); 17 July 2009 (*b*); 23 July 2011 (*c*). (*d*) – (*f*) Simulated tidal current field for images from 28 July 2007 (*d*); 17 July 2009 (*e*); 23 July 2011 (*f*) accordingly. Colour bar: current intensity (m s^{-1}). Black arrow: current direction. Black circle: position where SPMC clearly changed near the centre of the bay.

July 2011 as examples). Figure 4 shows three high-SPMC areas in the study area, the first to the west of Hangzhou Bay, the second in a shallow-water sandbar to the south of the bay, and the third to the northeast of the bay close to the mouth of the Yangtze River. The current fields for each satellite image show that when the tidal currents flow inward (westwards) (Figure 4(*d*)), the central part of the bay shows relatively higher SPMC values (black circles in Figure 4(*a*)). When the tidal currents flow outwards (eastwards) (Figure 4(*e*) and (*f*)), the central area of the bay shows relatively low SPMC values (black circles in Figure 4(*b*) and (*c*)).

When the current flows past a bridge, pier-induced flow (comb-like) can be seen at the rear of the bridge in Landsat-5 TM enhanced images (Figure 2(*c*)). This comb-like flow can be used to estimate the direction of local water currents. We define comb-like flow side as downstream, and the opposite as upstream.

In general, for the HBB area, SPMC values near the centre of the bridge were lower than at the two ends (Figures 5(*a*), (*c*), and (*e*)). For JTB, higher SPMC valuess were clearly observed at the western end of the bridge compared with the eastern end. The average SPMC was 300 mg l^{-1}, and the maximum in most cases was around 750 mg l^{-1} (Figure 5(*b*), (d), and (f)). SPMC analysis was performed on 11 images although only three example images are presented here. These SPMC levels show highly turbid water. Obvious differences in SPMC were observed between the upstream and downstream aspects of the bridges.

3.3.2. *Increased SPMC downstream of the bridges*

SPMC increased downstream of the HBB and JTB by 3–60% (the ratio between downstream and upstream SPMC) (Figure 6(*a*)). Incremental values of between 8.40–176.29 mg l^{-1} were found at almost all paired sampling points within 0.3 km downstream from the bridges, with only a few points showing SPMC decreasing downstream.

In general, downstream SPMC downstream was positively correlated with upstream SPMC (Figure 6(*b*)) but the variation cannot be ignored. SPMC increased significantly for upstream water with SPMC >300 mg l^{-1}. The more turbid the water upstream, the less SPMC increased in amplitude downstream (Figure 6(*a*)). The spatial region of increased SPMC extended to approximately 2.0–6.5 km downstream (Figure 7 (Transects 1–2), (Transect 4), and (Transects 7–8)). Thirty transects were analysed on 11 images, from which we selected eight.

3.3.3. *Decreased SPMC downstream of the bridges*

For high-turbidity water upstream (SPMC >400 mg l^{-1}, occasionally >350 mg l^{-1}), SPMC decreased by 2.0–17.5% (12.60–62.98 mg l^{-1}) (as seen from the points below the zero line in Figure 6(*a*)) 0.3 km or more downstream from the piers (Figure 7 (Transect 3) and 7 (Transect 5)).

Under upstream turbid water conditions, decreased SPMC was observed approximately 0.3–6.5 km downstream from the bridge, but is significant and clearly detectable at 1.5 km and beyond (Figure 7 (Transect 3), 7 (Transect 5), and 7 (Transect 6)).

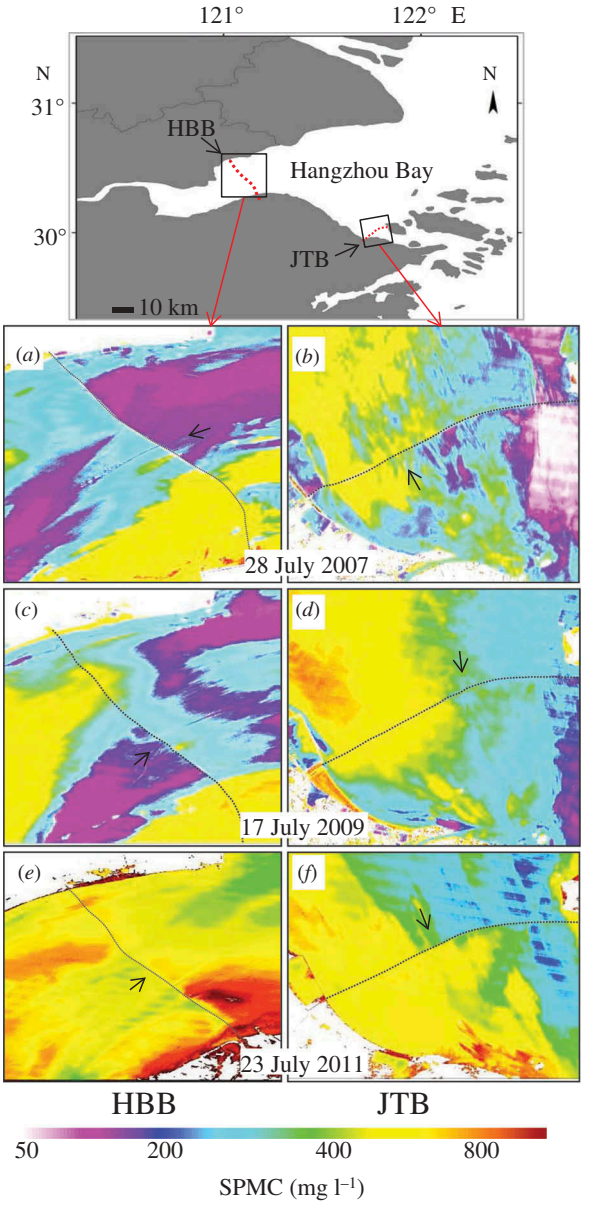

Figure 5. Local surface SPMC distribution near HBB and JTB retrieved from Landsat TM images on 28 July 2007 (*a*) – (*b*); 17 July 2009 (*c*)–(*d*); 23 July 2011 (*e*)–(*f*). Black and red broken lines: HBB and JTB, respectively. Black arrows: tidal current direction.

4. Discussion

4.1. Applicability of novel 'SPM-CT'

Both the red and NIR band are sensitive to SPMC in high-turbid water (Figure 2(*a*)). The NIR single band was used to build a suspended sediment inverse model in our prior study (Cai, Tang, and Li 2015a). Considering that the red band (red lines in Figure 2(*b*)) is more

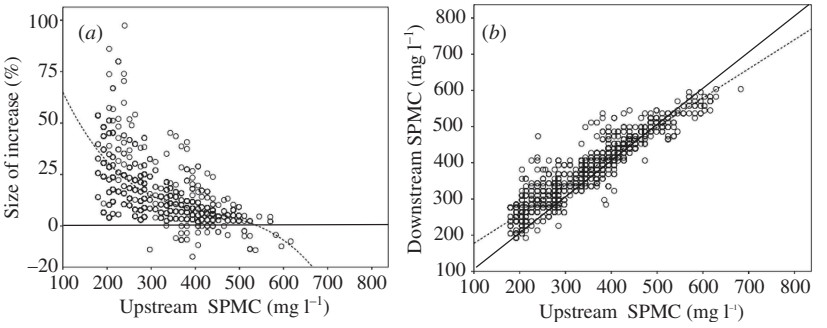

Figure 6. (*a*) Regression analysis between upstream water SPMC and increase in SPMC downstream (sampled 0.3 km downstream during rising and ebbing tides). The points linking unchanged SPMC are distributed on a horizontal line; positive values denote SPMC increase and negative values denote SPMC decrease. (*b*) Regression analysis of upstream and downstream SPMC sampled 0.3 km downstream during rising and ebbing tides.

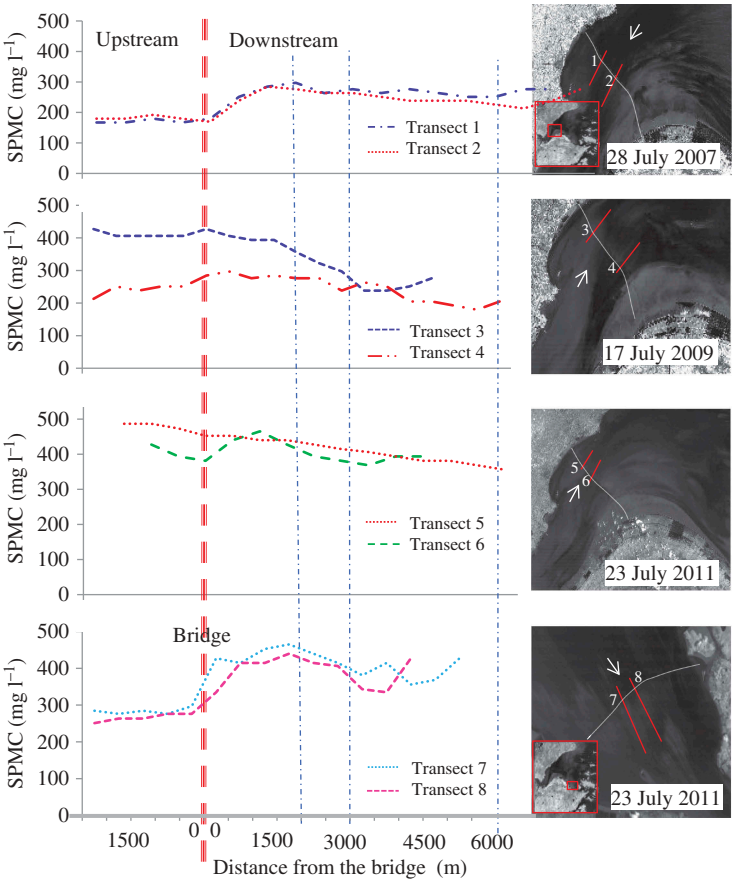

Figure 7. SPMC along transects sampled from SPMC maps obtained from Landsat TM images on 28 July 2007 (1–2); 17 July 2009 (3–4); 23 July 2011(5–8). (Transects 1–6: HBB; Transects 7– 8: JTB). Vertical red dashed line to the left and white line to the right denote the bridges. White arrows: tidal current direction.

sensitive to suspended sediment than the NIR band in low-turbidity water (i.e. the R_{rs} value for the red band increases significantly with increase in SPMC while the NIR band is sensitive to SPMC in high-turbidity water), the reflectance value in the red and NIR bands combined can better reveal the difference in SPMC. We exploited these variations in reflectance in the NIR and red bands to establish the model 'SPM-CT'.

The 'SPM-CT'-derived SPMC distribution in this study is consistent with SPMC estimates in prior research (Li, Gao, and Wang 2010; Xie et al. 2013).

4.2. *Factors contributing to large-scale SPMC distribution*

The distribution of SPMC over the entire area of Hangzhou Bay is influenced mainly by the tidal currents, the topography, and fresh water runoff. The location of relatively high-SPMC areas (Figure 4(*a*)–(*c*)) is consistent with the three shallow parts (Cai et al. 2015b) of Hangzhou Bay. The freshwater runoff from the rivers Yangtze and Qiantang carries suspended sediment into Hangzhou Bay (Han, Dai, and Li 2003). SPM is always deposited during the turning phase of the tide when tidal currents slacken (Hu et al. 2009), with the maximum concentration lagging behind the peak tide current and with the vertical distribution of SPMC being low on top and high below (Chen and Wang 2008).

4.3. *SPMC is affected by the interaction between current and bridge piers*

In the waters surrounding the bridges, SPMC distribution is significantly influenced by their presence, in two ways: (i) blocking the current carrying upstream SPM, thereby promoting sediment deposition downstream; and (ii) inducing local scouring near the bridge, resulting in sediment resuspension.

4.3.1. *The blocking role of bridge piers*

When bridge pier spacing is less than 150 m, the piers can significantly influence the current velocity by blocking it (Liu 2006; Pasiok and Stilger-SzydŁO 2010), resulting in reduced near the bridge (Qiao et al. 2011). Most of the piers on these two bridges are spaced about 50–90 m apart, except for a few near the main navigational route, which are spaced wider than 150 m. Nearly 7% of the cross-sectional area of the bay is blocked by the bridges' piers, promoting SPM deposition that can be observed approximately 0.3–6.5 km from the bridges.

4.3.2. *The resuspension role of the bridges*

Because of the interaction of the currents with piers, local scouring can be generated from downwelling in front of the pier, the wake vortex behind, and the vertical vortex alongside, thereby resuspending the particles from the scour hole downstream (Baker 1979; Pasiok and Stilger-SzydŁO 2010; Unger and Hager 2007), resulting in increased SPMC (Figures 5–7). SPMC and the hydrodynamic conditions of the currents, the bathymetric characteristics, the makeup of the seabed (e.g., clay or sand), the pier condition, and even Reynolds numbers can all influence local scour around a bridge pier (Debnath and Chaudhuri 2011; Raudkivi and Ettema 1983; Ting et al. 2001) and contribute to sediment resuspension.

A combination of deposition and resuspension resulted in the changes in SPMC downstream. Sometimes the variation in SPMC was not obvious downstream compared

with upstream because (i) the pier spacing (located on the main navigational route) was wider than 150 m (Liu 2006), and (ii) a balance exists whereby deposition is offset by resuspension. The offset buffer zone (deposition and resuspension interaction region) for SPMC is approximately 3.0–6.5 km downstream from the bridge (sometimes >7 km; downstream region to the left in Figure 7), with SPMC gradually declining. It is an interesting suggestion that there seems to be a deposition belt forming on the seabed approximately 2–5 km downstream from the bridge. As the upstream and downstream waters near the bridges change with the direction of tidal current, there are two belts parallel to the bridge, one upstream and one downstream, extending 2–5 km from the bridge, where sediment tends to be deposited. One study suggested the presence of such belts at other bridges (Qiao et al. 2011).

5. Summary and conclusions

In this study, we derived a new model 'SPM-CT' to retrieve SPMC from Landsat Thematic Mapper data, using a combination of the red and NIR bands. This novel model is capable of estimating SPMC in coastal waters, especially in SPM-dominant water such as Hangzhou Bay.

SPMC in the vicinity of HBB and JTB was significantly different on opposite sides of the bridges. Within 0.3 km downstream of the bridges, SPMC mostly increased by 3–60%. When SPMC was low upstream, it tended to increase downstream, extending approximately 3.0–6.5 km. Under conditions of high (>400 mg l^{-1}) SPMC upstream, we observed a decrease in SPMC 0.3–6.5 km downstream, which became more marked about 1.5 km from the bridges.

The impacts of bridges on SPMC in the surrounding waters are mainly as a result of their dual role: (i) blocking the current carrying upstream SPM, thereby promoting sediment deposition downstream; and (ii) inducing local scouring near the bridge, thereby leading to sediment resuspension. The offset buffer zone (deposition and resuspension interaction region) for SPMC is approximately 3.0–6.5 km downstream from the bridge, with SPMC gradually declining. A deposition belt formed on the seabed at approximately 2–5 km downstream from the bridge. Downstream variation in SPMC is the net result of deposition and resuspension.

Acknowledgement

The Centre for Earth Observation and Digital Earth, Chinese Academy of Sciences, China, provided Landsat data.

Disclosure statement

No potential conflict of interest was reported by the authors.

Funding

This work was supported by the Key Project of National Natural Sciences Foundation of China [grant number NNSFC 41430968]; the Key Project of Collaborative Innovation Centre for 21st-Century Maritime Silk Road Studies [grant number 2015HS05]; the Visiting Fellowship Programme of Chinese Academy of Sciences; and the State Key Laboratory of Tropical Oceanography, South China Sea Institute of Oceanology [grant number 2013T1Z0048], [grant number LTO-OVFP-1501].

References

Amante, C., and B. W. Eakins 2009. "ETOPO1 1 Arc-Minute Global Relief Model: Procedures, Data Sources and Analysis." In *NOAA Technical Memorandum NESDIS NGDC-24. National Geophysical Data CenterMarine Geology and Geophysics Division*. 1–10. NOAA. doi:10.7289/V5C8276M.

Baker, C. 1979. "The Laminar Horseshoe Vortex." *Journal of Fluid Mechanics* 95 (02): 347–367. doi:10.1017/S0022112079001506.

Cai, L. N., D. L. Tang, and C. Y. Li. 2015a. An Investigation of Spatial Variation of Suspended Sediment Concentration Induced by a Bay Bridge Based on Landsat TM and OLI Data. *Advances in Space Research* 56: 293–303. doi:10.1016/j.asr.2015.04.015.

Cai, L. N., D. L. Tang, X. F. Li, H. Zheng, and W. Shao. 2015b. "Remote Sensing of Spatial-Temporal Distribution of Suspended Sediment and Analysis of Related Environmental Factors in Hangzhou Bay, China." *Remote Sensing Letters* 6 (8): 597–603. doi:10.1080/2150704X.2015.1062158.

Charou, E., M. Stefouli, D. Dimitrakopoulos, E. Vasiliou, and O. D. Mavrantza. 2010. "Using Remote Sensing to Assess Impact of Mining Activities on Land and Water Resources." *Mine Water and the Environment* 29 (1): 45–52. doi:10.1007/s10230-010-0098-0.

Chavez Jr, P. S. 1988. "An Improved Dark-Object Subtraction Technique for Atmospheric Scattering Correction of Multispectral Data." *Remote Sensing of Environment* 24 (3): 459–479. doi:10.1016/0034-4257(88)90019-3.

Chen, B., and K. Wang. 2008. "Suspended Sediment Transport in the Offshore near Yangtze Estuary." *Journal of Hydrodynamics, Series B* 20 (3): 373–381. doi:10.1016/S1001-6058(08)60070-0.

Chen, S. L., G. Zhang, and S. Yang. 2003. "Temporal and Spatial Changes of Suspended Sediment Concentration and Resuspension in the Yangtze River Estuary." *Journal of Geographical Sciences* 13 (4): 498–506. doi:10.1007/BF02837889.

Choi, J., Y. Park, B. Lee, J. Eom, J. Moon, and J. Ryu. 2014. "Application of the Geostationary Ocean Color Imager (GOCI) to Mapping the Temporal Dynamics of Coastal Water Turbidity." *Remote Sensing of Environment* 146: 24–35. doi:10.1016/j.rse.2013.05.032.

Cloern, J. E. 1987. "Turbidity as a Control on Phytoplankton Biomass and Productivity in Estuaries." *Continental Shelf Research* 7 (11–12): 1367–1381. doi:10.1016/0278-4343(87)90042-2.

Debnath, K., and S. Chaudhuri. 2011. "Effect of Suspended Sediment Concentration on Local Scour around Cylinder for Clay–Sand Mixed Sediment Beds." *Engineering Geology* 117 (3–4): 236–245. doi:10.1016/j.enggeo.2010.11.003.

Dekker, A. G., R. Vos, and S. Peters. 2002. "Analytical Algorithms for Lake Water TSM Estimation for Retrospective Analyses of TM and SPOT Sensor Data." *International Journal of Remote Sensing* 23 (1): 15–35. doi:10.1080/01431160010006917.

Dewidar, K., and A. Khedr. 2001. "Water Quality Assessment with Simultaneous Landsat-5 TM at Manzala Lagoon, Egypt." *Hydrobiologia* 457 (1/3): 49–58. doi:10.1023/A:1012281416096.

Doxaran, D., N. Cherukuru, and S. J. Lavender. 2006. "Apparent and Inherent Optical Properties of Turbid Estuarine Waters: Measurements, Empirical Quantification Relationships, and Modeling." *Applied Optics* 45 (10): 2310–2324. doi:10.1364/AO.45.002310.

Doxaran, D., J.-M. Froidefond, S. Lavender, and P. Castaing. 2002. " Spectral Signature of Highly Turbid Water Application with SPOT Data to Quantify Suspended Particulate Matter Concentration." *Remote Sensing of Environment* 81 (1): 149–161. doi:10.1016/S0034-4257(01)00341-8.

ENVI. 1997. *ENVI User's Guide*. Chap. 1–10. Lafayette, CO: Better Solutions Consulting Limited Liability Company.

Fan, H., H. Huang, and J. Tang. 2007. "Spectral Signature of Waters in Huanghe Estuary and Estimation of Suspended Sediment Concentration from Remote Sensing Data." *Geomatics and Information Science of Wuhan University* 32 (7): 601–604. doi:10.13203/j.whugis2007.07.009.

Fan, W., and J. Song. 2014. "A Numerical Study of the Seasonal Variations of Nutrients in the Changjiang River Estuary and Its Adjacent Sea Area." *Ecological Modelling* 291: 69–81. doi:10.1016/j.ecolmodel.2014.07.026.

Firat, M., and M. Gungor. 2009. "Generalized Regression Neural Networks and Feed Forward Neural Networks for Prediction of Scour Depth around Bridge Piers." *Advances in Engineering Software* 40 (8): 731–737. doi:10.1016/j.advengsoft.2008.12.001.

Hadjimitsis, D. G., M. G. Hadjimitsis, C. Clayton, and B. A. Clarke. 2006. "Determination of Turbidity in Kourris Dam in Cyprus Utilizing Landsat TM Remotely Sensed Data." *Water Resources Management* 20 (3): 449–465. doi:10.1007/s11269-006-3089-y.

Hale, G. M., and M. R. Querry. 1973. "Optical Constants of Water in the 200-Nm to 200-Mm Wavelength Region." *Applied Optics* 12 (3): 555–563. doi:10.1364/AO.12.000555.

Han, Z., Z. Dai, and G. Li. 2003. *Regulation and Exploitation of Qiantang Estuary*. Beijing: China Water Power Press.

He, X. Q., Y. Bai, D. L. Pan, N. L. Huang, X. Dong, J. S. Chen, C. T. A. Chen, and Q. F. Cui. 2013. "Using Geostationary Satellite Ocean Color Data to Map the Diurnal Dynamics of Suspended Particulate Matter in Coastal Waters." *Remote Sensing of Environment* 133: 225–239. doi:10.1016/j.rse.2013.01.023.

Hu, C., Z. Chen, T. D. Clayton, P. Swarzenski, J. C. Brock, and F. E. Muller–Karger. 2004. "Assessment of Estuarine Water-Quality Indicators Using MODIS Medium-Resolution Bands: Initial Results from Tampa Bay, FL." *Remote Sensing of Environment* 93 (3): 423–441. doi:10.1016/j.rse.2004.08.007.

Hu, R., J. Wu, L. Zhu, and F. Ma. 2009. "Suspended Sediment Transport and Deposition in the Zhoushan Archipelago Sea Area." *Journal of Ocean University of China* 8 (4): 343–351. doi:10.1007/s11802-009-0343-y.

Jilan, S., and W. Kangshan. 1989. "Changjiang River Plume and Suspended Sediment Transport in Hangzhou Bay." *Continental Shelf Research* 9 (1): 93–111. doi:10.1016/0278-4343(89)90085-X.

Li, J., S. Gao, and Y. Wang. 2010. "Delineating Suspended Sediment Concentration Patterns in Surface Waters of the Changjiang Estuary by Remote Sensing Analysis." *Acta Oceanologica Sinica* 29 (4): 38–47. doi:10.1007/s13131-010-0049-4.

Li, X., and H. Guo. 2014. "Remote Sensing of the China Seas." *International Journal of Remote Sensing* 35 (11–12): 3919–3925. doi:10.1080/01431161.2014.920599.

Liu, H. 2006. "Hydrodynamic Problems Associated with Construction of Sea-Crossing Bridges." *Journal of Hydrodynamics, Series B* 18 (3): 13–18. doi:10.1016/S1001-6058(06)60023-1.

Liu, S., Y. Liu, G. Yang, S. Qiao, C. Li, Z. Zhu, and X. Shi. 2012. "Distribution of Major and Trace Elements in Surface Sediments of Hangzhou Bay in China." *Acta Oceanologica Sinica* 31 (4): 89–100. doi:10.1007/s13131-012-0223-y.

MatAmin, A. R., F. Ahmad, M. Mamat, M. Rivaie, and K. Abdullah. 2012. "Sediment Variation along the East Coast of Peninsular Malaysia." *Ecological Questions* 16 (1): 99–107. doi:10.12775/v10090-012-0010-6.

Mayer, L. M., R. G. Keil, S. A. Macko, S. B. Joye, K. C. Ruttenberg, and R. C. Aller. 1998. "Importance of Suspended Participates in Riverine Delivery of Bioavailable Nitrogen to Coastal Zones." *Global Biogeochemical Cycles* 12 (4): 573–579. doi:10.1029/98GB02267.

Mustak, S. 2013. "Correction of Atmospheric Haze in Resourcesat-1 LISS-4 MX Data for Urban Analysis: An Improved Dark Object Subtraction Approach." *International Archives of the Photogrammetry, Remote Sensing and Spatial Information Sciences* XL-1/W3: 5.

Pasiok, R., and E. Stilger-SzydŁO. 2010. "Sediment Particles and Turbulent Flow Simulation around Bridge Piers." *Archives of Civil and Mechanical Engineering* 10 (2): 67–79. doi:10.1016/S1644-9665(12)60051-X.

Pattiaratchi, C., P. Lavery, A. Wyllie, and P. Hick. 1994. "Estimates of Water Quality in Coastal Waters Using Multi-Date Landsat Thematic Mapper Data." *International Journal of Remote Sensing* 15 (8): 1571–1584. doi:10.1080/01431169408954192.

Prasad, A. K., and R. P. Singh. 2009. "Validation of MODIS Terra, AIRS, NCEP/DOE AMIP-II Reanalysis-2, and AERONET Sun Photometer Derived Integrated Precipitable Water Vapor Using Ground-Based GPS Receivers over India." *Journal of Geophysical Research: Atmospheres (1984–2012)* 114 (D5). doi:10.1029/2008JD011230.

Qiao, S., D. L. Pan, X. Q. He, and Q. F. Cui. 2011. "Numerical Study of the Influence of Donghai Bridge on Sediment Transport in the Mouth of Hangzhou Bay." *Procedia Environmental Sciences* 10 (2011): 408–413. doi:10.1016/j.proenv.2011.09.067.

Qiu, Z. F. 2013. "A Simple Optical Model to Estimate Suspended Particulate Matter in Yellow River Estuary." *Optics Express* 21 (23): 27891–27904. doi:10.1364/oe.21.027891.
Raudkivi, A. J., and R. Ettema. 1983. "Clear-Water Scour at Cylindrical Piers." *Journal of Hydraulic Engineering* 109 (3): 338–350. doi:10.1061/(ASCE)0733-9429(1983)109:3(338).
Richter, R. 1990. "A Fast Atmospheric Correction Algorithm Applied to Landsat TM Images." *International Journal of Remote Sensing* 11 (1): 159–166. doi:10.1080/01431169008955008.
Shen, F., W. Verhoef, Y. Zhou, M. S. Salama, and X. Liu. 2010. "Satellite Estimates of Wide-Range Suspended Sediment Concentrations in Changjiang (Yangtze) Estuary Using MERIS Data." *Estuaries and Coasts* 33 (6): 1420–1429. doi:10.1007/s12237-010-9313-2.
Shengquan, G., G. Guohui, and W. Yuhen. 1993. "Distributional Features and Fluxes of Dissolved Nitrogen, Phosphorus and Silicon in the Hangzhou Bay." *Marine Chemistry* 43 (1–4): 65–81. doi:10.1016/0304-4203(93)90216-B.
Shin, J. H., and H. I. Park. 2010. "Development and Application of a 3-Dimensional Scour Monitoring System for Sea-Crossing Bridge Piers." *International Journal of Offshore and Polar Engineering* 20 (4): 292–297.
Song, Y., and D. Haidvogel. 1994. "A Semi-Implicit Ocean Circulation Model Using A Generalized Topography-Following Coordinate System." *Journal of Computational Physics* 115 (1): 228–244. doi:10.1006/jcph.1994.1189.
Tang, D., H. Kawamura, M. Lee, and T. Dien. 2003a. "Seasonal and Spatial Distribution of Chlorophyll-*A* Concentrations and Water Conditions in the Gulf of Tonkin, South China Sea." *Remote Sensing of Environment* 85 (4): 475–483. doi:10.1016/S0034-4257(03)00049-X.
Tang, D., D. Kester, I.-H. Ni, Y. Qi, and H. Kawamura. 2003b. "In Situ and Satellite Observations of a Harmful Algal Bloom and Water Condition at the Pearl River Estuary in Late Autumn 1998." *Harmful Algae* 2: 89–99. doi:10.1016/S1568-9883(03)00021-0.
Tang, D. L., I. Ni, F. Müller-Karger, and Z. Liu. 1998. "Analysis of Annual and Spatial Patterns of CZCS-Derived Pigment Concentration on the Continental Shelf of China." *Continental Shelf Research* 18 (12): 1493–1515. doi:10.1016/S0278-4343(98)00039-9.
Teillet, P., and G. Fedosejevs. 1995. "On the Dark Target Approach to Atmospheric Correction of Remotely Sensed Data." *Canadian Journal of Remote Sensing* 21 (4): 374–387. doi:10.1080/07038992.1995.10855161.
Ting, F. C., J.-L. Briaud, H. Chen, R. Gudavalli, S. Perugu, and G. Wei. 2001. "Flume Tests for Scour in Clay at Circular Piers." *Journal of Hydraulic Engineering* 127 (11): 969–978. doi:10.1061/(ASCE)0733-9429(2001)127:11(969).
Unger, J., and W. H. Hager. 2007. "Down-Flow and Horseshoe Vortex Characteristics of Sediment Embedded Bridge Piers." *Experiments in Fluids* 42 (1): 1–19. doi:10.1007/s00348-006-0209-7.
Wang, F., B. Zhou, X. Liu, G. Zhou, and K. Zhao. 2012. "Remote-Sensing Inversion Model of Surface Water Suspended Sediment Concentration Based on in Situ Measured Spectrum in Hangzhou Bay, China." *Environmental Earth Sciences* 67 (6): 1669–1677. doi:10.1007/s12665-012-1608-0.
Warrick, J., L. Mertes, D. Siegel, and C. Mackenzie. 2004. "Estimating Suspended Sediment Concentrations in Turbid Coastal Waters of the Santa Barbara Channel with Seawifs." *International Journal of Remote Sensing* 25 (10): 1995–2002. doi:10.1080/01431160310001619535.
Webster, T., and C. Lemckert. 2002. "Sediment Resuspension within a Microtidal Estuary/Embayment and the Implication to Channel Management." *Journal of Coastal Research* 36: 753–759.
Xie, D., Z. Wang, S. Gao, and H. De Vriend. 2009. "Modeling the Tidal Channel Morphodynamics in a Macro-Tidal Embayment, Hangzhou Bay, China." *Continental Shelf Research* 29 (15): 1757–1767. doi:10.1016/j.csr.2009.03.009.
Xie, D.-F., S. Gao, Z.-B. Wang, and C.-H. Pan. 2013. "Numerical Modeling of Tidal Currents, Sediment Transport and Morphological Evolution in Hangzhou Bay, China." *International Journal of Sediment Research* 28 (3): 316–328. doi:10.1016/S1001-6279(13)60042-6.
Zhang, X. F., F. Hu, J. Zhang, and D. L. Tang. 2014. "Northward Drift of Suspended Sediments in the Yangtze Estuary in Spring." *International Journal of Remote Sensing* 35 (11–12): 4114–4126. doi:10.1080/01431161.2014.916455.
Zhou, W., S. Wang, Y. Zhou, and A. Troy. 2006. "Mapping the Concentrations of Total Suspended Matter in Lake Taihu, China, Using Landsat-5 TM Data." *International Journal of Remote Sensing* 27 (6): 1177–1191. doi:10.1080/01431160500353825.